Power-Law Spin Correlations in the Pyrochlore Antiferromagnet $Tb_2Ti_2O_7$

T. Fennell,[1,*] M. Kenzelmann,[2] B. Roessli,[1] M. K. Haas,[3] and R. J. Cava[3]

[1]*Laboratory for Neutron Scattering, Paul Scherrer Institut, 5232 Villigen PSI, Switzerland*
[2]*Laboratory for Developments and Methods, Paul Scherrer Institut, 5232 Villigen PSI, Switzerland*
[3]*Department of Chemistry, Princeton University, Princeton, New Jersey 08540, USA*

(Received 23 December 2011; revised manuscript received 19 March 2012; published 3 July 2012)

We investigate the low-temperature state of the rare-earth pyrochlore $Tb_2Ti_2O_7$ using polarized neutron scattering. $Tb_2Ti_2O_7$ is often described as an antiferromagnetic spin liquid with spin correlations extending over lengths comparable to individual tetrahedra of the pyrochlore lattice. We confirm this picture at 20 K but find that at 0.05 K the data contain evidence of pinch-point scattering, suggesting that the low temperature state of $Tb_2Ti_2O_7$ has power-law spin correlations.

DOI: 10.1103/PhysRevLett.109.017201 PACS numbers: 75.50.Ee, 75.10.Jm, 75.25.−j, 75.47.Lx

Spin correlations with power-law decay are usually associated with a critical point, but stable phases with power-law correlations may exist in frustrated magnets [1]. Such phases are interesting, because they represent model materials where short-range interactions and local constraints lead to emergent symmetries and fractional quasiparticles [1–5]. For example, in a spin ice, spin configurations that respect a local ice-rule constraint give rise to dipolar (i.e., $1/r^3$) spin correlations [6,7] and emergent magnetic monopoles [4]. Dipolar correlations are identified in scattering experiments by the existence of distinctive sharp and anisotropic features known as pinch points [8,9].

$Tb_2Ti_2O_7$ is a particularly interesting frustrated magnet [10]. Like the spin ice materials, it contains rare-earth ions that form corner-shared tetrahedra and have an Ising doublet ground state, so at low temperatures the magnetic moments are constrained to the trigonal (or $\langle 111 \rangle$) axes. However, the effective interactions are antiferromagnetic, not ferromagnetic as in the spin ices, so a different ground state is expected. Measurements of the local susceptibility ellipsoid show that $\chi_{\parallel\langle 111\rangle}/\chi_{\perp\langle 111\rangle} \sim 10$ at $T = 1.7$ K [11], and $\Theta_{\mathrm{CW}} = -19$ K, which should cause long-range ordering at $T_N \sim 1$ K [10]. However, no ordering is observed down to 0.05 K. Instead, diffuse neutron scattering measurements show a liquidlike $|\mathbf{Q}|$-dependence in powders (at 2.5 K) and a broad checkerboard pattern in single crystals (at 9 K). Both are well described by a model of isotropic spins correlated antiferromagnetically on a single tetrahedron [12] [see Fig. 2(i)]. Measurements at $T = 0.4$ and 0.05 K were also interpreted in terms of small correlated spin clusters (heptamer and tetrahedron, respectively) [13,14]. Spin dynamics can be detected at these temperatures by neutron scattering [13,14] and μ-SR techniques [15], so it was suggested that the ground state is a spin liquid.

The absence of classical order represents a long-standing theoretical challenge and has led to theories incorporating quantum fluctuations, again with calculations spanning a single tetrahedron [16,17]. All such calculations reproduce the checkerboard pattern, which is regarded as defining the character of the spin liquid state. One suggestion is that three-body exchange via virtual crystal field excitations repositions $Tb_2Ti_2O_7$ from a classical antiferromagnet to a "quantum spin ice," in which the ground state of a single tetrahedron is a superposition of 2-in–2-out states [16]. Another proposal involves splitting of the ground state doublet of the Tb^{3+} ions by a structural distortion [18]. Strong magnetoelastic effects exist in $Tb_2Ti_2O_7$, as manifested by anisotropic strain broadening [19], dielectric anomalies [20], and negative thermal expansion in the spin liquid state [19,21], but evidence for the splitting and associated symmetry lowering is not definitive [13,22–24].

In this Letter we cannot detect any departure from the cubic pyrochlore structure. We do not investigate the crystal field ground state, but use the measured spin anisotropy [11] as an experimental fact, taking advantage of it in order to investigate two spin correlation functions. We find evidence of pinch points, and therefore power-law spin correlations, in both. Our results demonstrate that spin correlations in $Tb_2Ti_2O_7$ extend over larger distances than previously observed, suggesting the presence of a hitherto unknown organizing principle, similar to the ice rules in spin ice.

The sample was a single crystal of $Tb_2Ti_2O_7$ weighing 7.2 g, grown in a floating zone furnace and annealed under argon to obtain a uniform dark red color. The crystal was aligned with the $[1\bar{1}0]$ direction vertical (within 1°) giving a horizontal scattering plane containing (h,h,l) wave vectors. We used the D7 [25] spectrometer at the ILL to map reciprocal space in two polarization channels, z (non-spin-flip) and z' (spin-flip). This process allows us to distinguish correlations among spin components that are perpendicular to the scattering plane from those that lie in it, which we call M_z and M_y, respectively (see Fig. 1). Standard corrections for polarization and detector efficiency (amorphous silica and vanadium samples, respectively) were made.

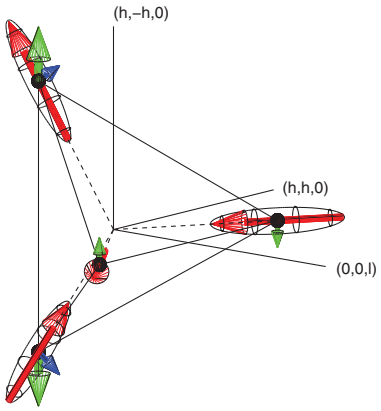

FIG. 1 (color). Experimental coordinates. The horizontal plane contains the scattering vectors **Q** [of type (h,h,l)]. The spin components are $M_x \parallel \mathbf{Q}$; M_z, vertical; and M_y, mutually perpendicular. Spin components perpendicular to both **Q** and the neutron polarization vector (**P**) cause spin-flip scattering, while those perpendicular to **Q** but parallel to **P** cause non-spin-flip scattering. With $\mathbf{P}_z$, correlations among in-plane (M_y) and out-of-plane (M_z) components can be distinguished. In $Tb_2Ti_2O_7$, the finite spin anisotropy indicated by the ellipsoids allows both M_y and M_z components at all four sites, and our calculations employ large $\langle 111 \rangle$ and small transverse components to model this. The M_y correlations are dominated by "2-in–2-out" ice-rule components (red) and the M_z correlations by "2-up–2-down" (green) ice-rule configurations [30] that mix $\langle 111 \rangle$ (red) and transverse (blue) contributions. The illustration is schematic, and the ratio of $\langle 111 \rangle$ to transverse components used in the calculations is 1:0.2.

Spin and isotope incoherent contributions obtained from a full xyz measurement at 100 K were subtracted, leaving only contributions from M_z plus nuclear Bragg scattering, or M_y. In addition, the low-temperature diffuse scattering maps have been divided by the measurements at 100 K to normalize a rotation-dependent intensity variation. This process also removes the magnetic form factor dependence and nuclear Bragg peaks. Because D7 integrates over energy transfers (up to the incident energy of 3.55 meV), we also used the TASP triple axis spectrometer at the PSI to study specific features as a function of wave vector and energy transfer. We measured six polarization channels (z, z'; x, x'; and y, y') to isolate M_y and M_z contributions. TASP was configured with a remnant supermirror polarizer and analyzer (80′ collimation), MuPAD [26] for polarization control, and $k_f = 1.3$ Å^{-1}, giving an energy resolution of 0.15 meV (FWHM).

Figure 2 shows diffuse scattering maps. At 20 K we recover almost exactly the checkerboard pattern in both the M_y and M_z scattering. As the temperature is decreased, the pattern evolves significantly. In the M_y channel, armlike features along the $\langle h, h, h \rangle$ directions appear, and sharp constrictions in the diffuse scattering around (0,0,2), (1,1,1), and (2,2,2) develop. At each of these points, the sharpening is perpendicular to the reciprocal lattice vector. In the M_z channel, the checkerboard evolves into butterfly-shaped features at (0,0,2) and (2,2,0). In this case, the sharpening is always parallel to (0,0,l) and less developed. Unpolarized experiments would have observed the sum of these two channels and, although features such as the $\langle h, h, h \rangle$ arms are visible in other data sets [13], they seem to have been overlooked in previous interpretations. It is not possible to determine the absolute strength of the M_z and M_y fluctuations from these measurements, but in Fig. 2(d) we show their ratio, I_{M_z}/I_{M_y}. This ratio suggests that the magnitudes of the M_z and M_y fluctuations are similar, and a combination of both is required to describe the magnetic properties of $Tb_2Ti_2O_7$. Figure 2(d) also implies that the M_z correlations are shorter-ranged and, as a consequence, the scattering is more diffuse (hence, the ratio is dominated by M_z in regions where there is little contribution from M_y). This result is also implicit in the broad features of Fig. 2(f), as compared to the detailed structures of Fig. 2(a).

The evolution of the diffuse scattering on cooling can be examined by making cuts through the data, as in Fig. 3. At 20 K, the scattering is very similar in both channels, so $M_y \approx M_z$, and all cuts can be fitted by the isotropic single tetrahedron model. Here, $Tb_2Ti_2O_7$ can be described by continuous spins interacting antiferromagnetically and correlated over short distances. The M_y scattering sharpens along (h,h,2) [Fig. 3(a)] into a peak that (at 0.05 K) can be fitted with a Lorentzian on a Gaussian background [Fig. 2(a) shows this is a broad contribution to the diffuse scattering], giving a correlation length of $\xi = 8 \pm 1$ Å. Along (0,0,l) [Fig. 3(b)], a broad Lorentzian develops ($\xi = 2 \pm 0.2$ Å), indicating that the correlations are highly anisotropic (this is the sharp direction in M_z, again indicating correlations in M_z are shorter ranged than those in M_y). The $\langle h, h, h \rangle$ arms in the M_y scattering also develop into sharp peaks [Fig. 3(c)], with a correlation length of $\xi = 10 \pm 1$ Å at (1, 1, 1). Comparison of the temperature dependence of the intensity of these features above the general base level of scattering (i.e., $\Delta_I = I_{\mathbf{Q}} - I_{\mathbf{Q}'}$, where **Q** is the position of interest and $\mathbf{Q}'$ is a position with no feature at low temperature) shows that they evolve continuously out of the single tetrahedron pattern. Interestingly, as shown in Fig. 3(d), the sharp features in the scattering track the temperature dependence of the local spin anisotropy measured in Ref. [11]. This result suggests that the increasing spin anisotropy with decreasing temperature, due to the thermal depopulation of excited crystal field levels, plays a crucial role in giving rise to the observed low-temperature spin correlations.

Because $Tb_2Ti_2O_7$ is known to have significant spin dynamics, even at low temperature, it is possible that the diffuse scattering measurements contain a significant quantity of integrated inelastic scattering, which would complicate any interpretation. We investigated this in our

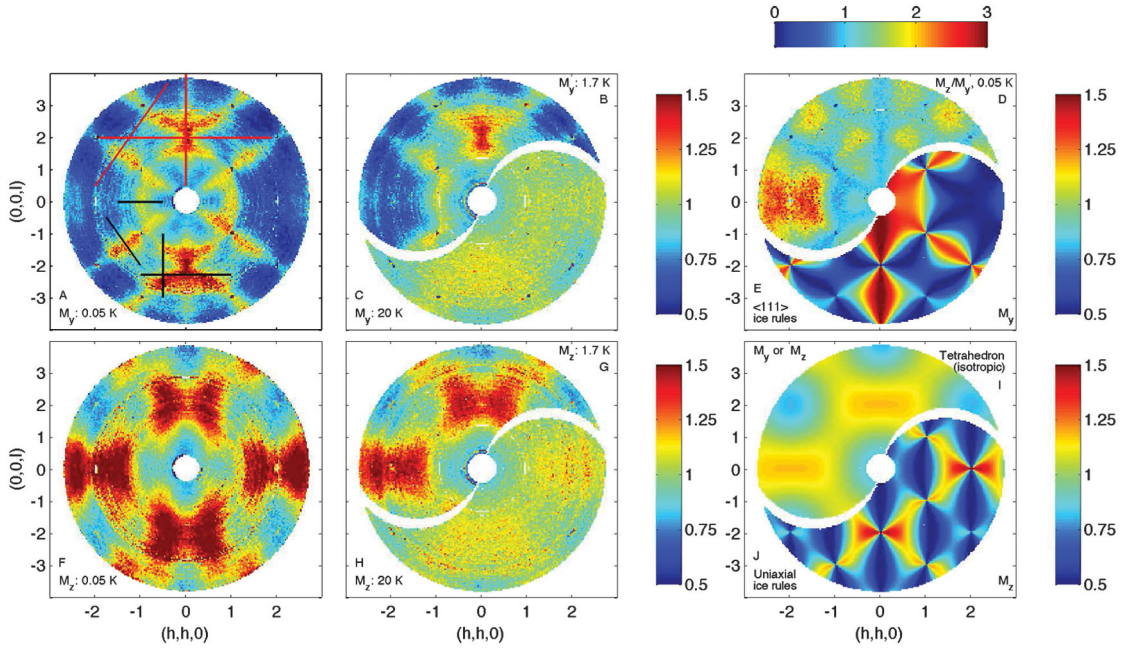

FIG. 2 (color). Diffuse scattering in $Tb_2Ti_2O_7$. The low-temperature state of $Tb_2Ti_2O_7$ has highly structured diffuse scattering with anisotropic sharp features, i.e., pinch points, in both the M_y (a) and M_z (f) channels. These can be seen to develop [(b) and (g)] below 20 K [(c) and (h)]. The ratio of the M_y and M_z intensities indicates the relative importance of the in- and out-of-plane components at different wave vectors (d). Model calculations show that dipolar correlations and 2-in–2-out spin configurations give rise to intensity in the M_y channel along (h,h,h) and $(0,0,l)$, with pinch points (d). Isotropic spins on single tetrahedra give the checkerboard pattern, which compares to either channel at 20 K (i). Uniaxial spins with unequal lengths (Fig. 1), 2-up–2-down ice rule, and dipolar correlations give butterflylike scattering (j). Red lines in A indicate cuts shown in Fig. 3; black lines are the scan directions of the energy-resolved measurements (Fig. 4).

triple-axis experiment. At 0.05 K, there is considerable quasielastic scattering of magnetic origin (Fig. 4), as in Ref. [13]. However, wave vector scans at different energy transfers [Figs. 4(a)–4(d)] show that elastic (up to the energy resolution of TASP) magnetic scattering due to M_z and M_y correlations captures precisely the wave vector dependence of the diffuse scattering maps [two scans are shown, but it is true for all four scans indicated on Fig. 2(a)], demonstrating that the maps are dominated by elastic scattering.

Although it seems unlikely that $Tb_2Ti_2O_7$ can be accurately described by classical theories, they may provide some clues about the spin correlations. In particular, the scattering in both channels sharpens about certain wave vectors in certain directions. This behavior is a defining feature of all pinch points, which unambiguously signal power-law (specifically, dipolar) correlations. In frustrated magnets on the pyrochlore lattice, these pinch points typically result from the propagation of a local ice-rule constraint. The M_y spin components appear to be controlled by a 2-in–2-out ice rule, and the M_z components by a poorly established 2-up–2-down condition.

To support this assertion, we make calculations based either on single tetrahedra or projection of the relevant spin components onto a general form for dipolar correlations on the pyrochlore lattice [7] (see also Supplemental Material [27]). The general distribution of the diffuse scattering is controlled by the structure factor of the spins on a single tetrahedron, while inclusion of the dipolar part produces the pinch points. For example, in Fig. 2(e), we show the full form for dipolar correlated 2-in–2-out $\langle 111 \rangle$ spins, which has arms of scattering along $(0, 0, l)$ and (h,h,h) modulated by sharp pinch points, while the single tetrahedron structure factor (not shown) just has broad arms in the same directions. Figure 2(j) shows the full calculation for uniaxial spins of two sizes obeying a 2-up–2-down ice rule (whose degeneracy is assumed to be unaffected by the two spin sizes), as illustrated in Fig. 1. The result is a pattern of butterfly shapes with sharp pinch points. Setting the lengths of $\langle 111 \rangle$ and perpendicular components in the ratio 1:0.2, in approximate agreement with the experimental susceptibility ellipsoid, and adding equal isotropic diffuse components to both channels [in Fig. 2(a), the M_y scattering never falls to zero] allows the features to be scaled to comparable intensity around (0,0,2), as shown in Fig. 2(d).

The application of these calculations is phenomenological, and it is clear that in their simplicity they will differ from the experimental data. However, several aspects of these calculations show important similarity to the experimental data. These features are the general distribution of scattering, and the orientation and position of the pinch points, all of which are strongly constrained by the

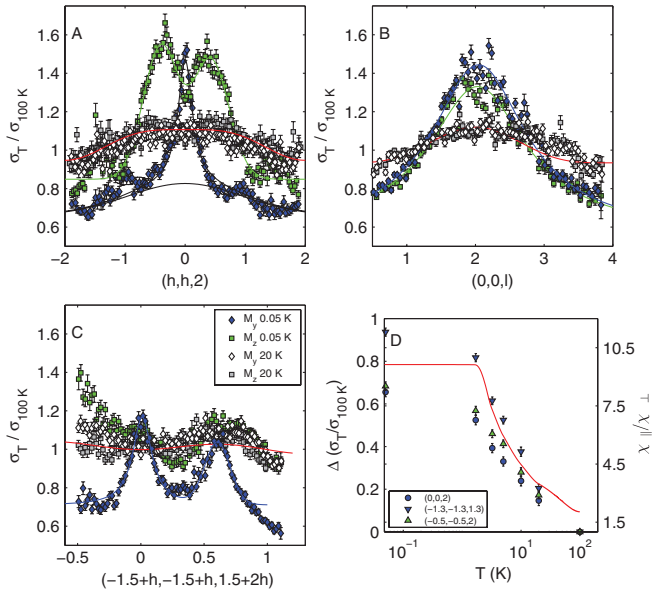

FIG. 3 (color). Temperature dependence of the diffuse scattering [cut directions in Fig. 2(a)]. At 20 K, the isotropic single tetrahedron model (red line) fits all data [(a),(b),(c)]. Sharp, anisotropic features develop at low temperatures. At 0.05 K, the M_y channel shows a Lorentzian peak perpendicular to (0,0,2) (a) and a broad one parallel to (0, 0, l) (b). The M_z channel has a two-peak structure perpendicular to and broad Lorentzian parallel to (0,0,l). The arms of scattering along (h, h, h) become strongly pronounced at low temperature (c). Integrated intensities from (0,0,2) (peak, M_y), (− 1.3,−1.3,1.3) (arm, M_y), and (− 0.5,−0.5,2) (butterfly, M_z) track the development of the spin anisotropy [(d), line from Ref. [11]].

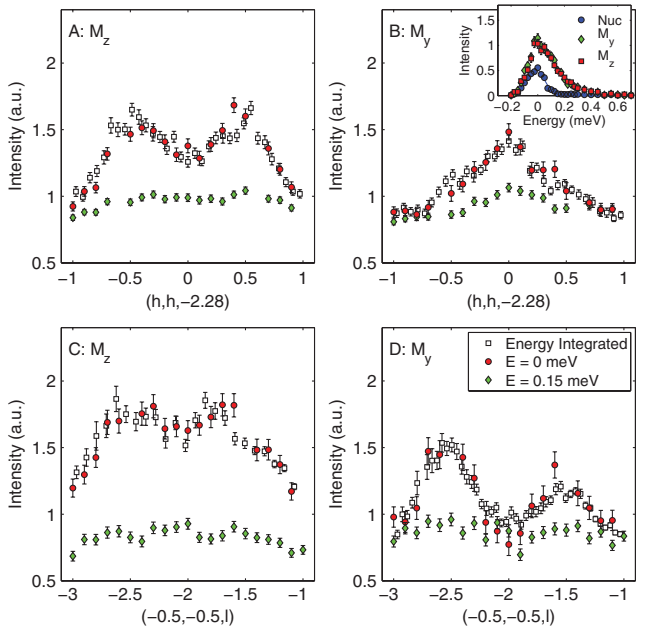

FIG. 4 (color). Comparison of energy-integrated and analyzed diffuse scattering measurements at 0.05 K. Quasielastic magnetic scattering with wave vector and polarization dependence extends to 0.4 meV (inset, nuclear scattering shows the resolution), but the M_z and M_y scattering for $\Delta E = 0$ along $\mathbf{Q} = (h, h, -2.28)$ [(a) and (b)] and (− 0.5,−0.5,l) [(c) and (d)] (scan directions shown in Fig. 2) overlays precisely cuts through the diffuse scattering maps of Fig. 2. Scaling and offsetting of the data are required because of the normalization of the diffuse scattering to a high-temperature data set.

existence of ice-rule correlations. For example, in the M_y channel, the absence of scattering around (h,h,0) and general extension of intensity along the (0,0,l) and (h,h,h) directions is a consequence of the 2-in–2-out structure factor, and the sharpening of the pinch points perpendicular to (0,0,2) and (1,1,1) is also specific to this geometry. In the M_z channel, the position and orientation of the pinch points result from considering uniaxial spin components of two sizes and contrast with the well-known arrangement of pinch points predicted in a conventional pyrochlore antiferromagnet [6,7]. Our experiment establishes the existence of two differently polarized spin correlation functions containing pinch points, and the calculations give a clear guidance about their origin. There are certainly important differences between the calculations and the experiment, such as the unrealistically sharp pinch points or intensity distribution around (0,0,3) and (0,0,0), on which we comment in more detail in the Supplemental Material [27], and which emphasize the need for more realistic theoretical studies.

The Hamiltonian proposed by Molavian *et al.* [16] has a superposition of 2-in–2-out spin configurations as a ground state in its quantum spin ice regime. A singly peaked structure in the diffuse neutron scattering along (h,h,2) is predicted to distinguish this state. We observe a single peak in M_y and a double peak in M_z [Fig. 3(a)], and the total (not shown) is a single peak, as predicted. The proposition of a two-singlet state [18] makes no predictions of the diffuse scattering at present, but it requires a new crystal field level at 0.1–0.2 meV, which we cannot distinguish from quasielastic scattering with the present resolution. Recent experiments also suggest an unknown transition occurs at $T \sim 0.15$–0.4 K [28], where our temperature dependence is not detailed.

Our experiments show that, at low temperature, $Tb_2Ti_2O_7$ has static power-law spin correlations that have more in common with ice models than liquidlike models. The evolution of this state accompanies the depopulation of excited crystal field levels, such that the appearance of structure in the diffuse scattering mirrors the elongation of the local susceptibility ellipsoid. It remains remarkable that there is no long-range ordering. Our experiments probe two orthogonal correlation functions and suggest that they contain pinch points of different forms, and that one (M_y) has a considerably longer correlation length than the other (M_z). The identification of spin textures with conjugate power-law correlations would appear consistent with a state supporting both emergent B and E fields, as in a

quantum spin ice [1,3,16]. We note that it is currently predicted that pinch points are not a characteristic of the quantum spin ice state [5], but other theories with correlations governed by different numbers of gauge fields are possible [29]. The identification of two sets of pinch points in $Tb_2Ti_2O_7$ should therefore provide an experimental catalyst for further examination of spin correlations in effective field theories of frustrated magnets, as well as providing a stringent test for theories of $Tb_2Ti_2O_7$.

We thank J. S. Gardner for advice on annealing $Tb_2Ti_2O_7$ crystals; P. M. McClarty, M. J. P. Gingras, M. Hermele, P. C. W. Holdsworth, and T. Roscilde for general discussions and S. T. Bramwell for detailed discussion of Ref. [7]; M. Zolliker, R. Ammer, and S. Turc for technical and cryogenics support; and A. L. Poole and D. F. McMorrow for comments on the manuscript. Neutron scattering experiments were carried out at the high flux reactor of the Institut Laue Langevin in Grenoble, France, and the continuous spallation neutron source SINQ at the Paul Scherrer Institut at Villigen PSI in Switzerland.

*tom.fennell@psi.ch

[1] C. L. Henley, Annu. Rev. Condens. Matter Phys. **1**, 179 (2010); L. Balents, Nature (London) **464**, 199 (2010).
[2] D. A. Huse, W. Krauth, R. Moessner, and S. L. Sondhi, Phys. Rev. Lett. **91**, 167004 (2003).
[3] M. Hermele, M. P. A. Fisher, and L. Balents, Phys. Rev. B **69**, 064404 (2004).
[4] C. Castelnovo, R. Moessner, and S. L. Sondhi, Nature (London) **451**, 42 (2008); R. Moessner and S. L. Sondhi, Phys. Rev. Lett. **105**, 166401 (2010).
[5] N. Shannon, O. Sikora, F. Pollmann, K. Penc, and P. Fulde, Phys. Rev. Lett. **108**, 067204 (2012).
[6] S. V. Isakov, K. Gregor, R. Moessner, and S. L. Sondhi, Phys. Rev. Lett. **93**, 167204 (2004).
[7] C. L. Henley, Phys. Rev. B **71**, 014424 (2005).
[8] R. Youngblood and J. D. Axe, Phys. Rev. B **17**, 3639 (1978); J. Skalyo, B. C. Frazer, and G. Shirane, *ibid.* **1**, 278 (1970); G. L. Paul, W. Cochran, W. J. L. Buyers, and R. A. Cowley *ibid.* **2**, 4603 (1970).
[9] T. Fennell, P. P. Deen, A. R. Wildes, K. Schmalzl, D. Prabhakaran, A. T. Boothroyd, R. J. Aldus, D. F. Mcmorrow, and S. T. Bramwell, Science **326**, 415 (2009); T. Fennell, S. T. Bramwell, D. F. Mcmorrow, P. Manuel, and A. R. Wildes, Nat. Phys. **3**, 566 (2007).
[10] J. S. Gardner, M. J. P. Gingras, and J. E. Greedan, Rev. Mod. Phys. **82**, 53 (2010).
[11] H. Cao, A. Gukasov, I. Mirebeau, P. Bonville, C. Decorse, and G. Dhalenne, Phys. Rev. Lett. **103**, 056402 (2009).
[12] J. S. Gardner, B. D. Gaulin, A. J. Berlinsky, P. Waldron, S. R. Dunsiger, N. P. Raju, and J. E. Greedan, Phys. Rev. B **64**, 224416 (2001).
[13] Y. Yasui, M. Kanada, M. Ito, H. Harashina, M. Sato, H. Okumura, K. Kakurai, and H. Kadowaki, J. Phys. Soc. Jpn. **71**, 599 (2002).
[14] J. S. Gardner, A. Keren, G. Ehlers, C. Stock, E. Segal, J. M. Roper, B. Fåk, M. B. Stone, P. R. Hammar, D. H. Reich, and B. D. Gaulin, Phys. Rev. B **68**, 180401(R) (2003).
[15] J. S. Gardner, S. R. Dunsiger, B. D. Gaulin, M. J. P. Gingras, J. E. Greedan, R. F. Kiefl, M. D. Lumsden, W. A. MacFarlane, N. P. Raju, J. E. Sonier, I. Swainson, and Z. Tun, Phys. Rev. Lett. **82**, 1012 (1999).
[16] H. R. Molavian, M. J. P. Gingras, and B. Canals, Phys. Rev. Lett. **98**, 157204 (2007).
[17] S. H. Curnoe, Phys. Rev. B **75**, 212404 (2007); **78**, 094418 (2008).
[18] P. Bonville, I. Mirebeau, A. Gukasov, S. Petit, and J. Robert, Phys. Rev. B **84**, 184409 (2011).
[19] J. P. C. Ruff, B. D. Gaulin, J. P. Castellan, K. C. Rule, J. P. Clancy, J. Rodriguez, and H. A. Dabkowska, Phys. Rev. Lett. **99**, 237202 (2007); J. P. C. Ruff, Z. Islam, J. P. Clancy, K. A. Ross, H. Nojiri, Y. H. Matsuda, H. A. Dabkowska, A. D. Dabkowski, and B. D. Gaulin, Phys. Rev. Lett. **105**, 077203 (2010).
[20] L. Mamsurova, K. Pigal'skii, N. Trusevich, and L. G. Shcherbakova, Sov. Phys. Solid State **27**, 978 (1985).
[21] K. Goto, H. Takatsu, T. Taniguchi, and H. Kadowaki, J. Phys. Soc. Jpn. **81**, 015001 (2012).
[22] I. Mirebeau, P. Bonville, and M. Hennion, Phys. Rev. B **76**, 184436 (2007).
[23] B. D. Gaulin, J. S. Gardner, P. A. McClarty, and M. J. P. Gingras, Phys. Rev. B **84**, 140402 (2011).
[24] Y. Chapuis, A. Yaouanc, P. Dalmas de Réotier, C. Marin, S. Vanishri, S. H. Curnoe, C. Vaju, and A. Forget, Phys. Rev. B **82**, 100402 (2010); S. W. Han, J. S. Gardner, and C. H. Booth, Phys. Rev. B **69**, 024416 (2004); O. Ofer, A. Keren, and C. Baines, J. Phys. Condens. Matter **19**, 145270 (2007); T. T. A. Lummen, I. P. Handayani, M. C. Donker, D. Fausti, G. Dhalenne, P. Berthet, A. Revcolevschi, and P. H. M. van Loosdrecht, Phys. Rev. B **77**, 214310 (2008).
[25] J. R. Stewart, P. P. Deen, K. H. Andersen, H. Schober, J.-F. Barthélémy, J. M. Hillier, A. P. Murani, T. Hayes, and B. Lindenau, J. Appl. Crystallogr. **42**, 69 (2008).
[26] M. Janoschek, S. Klimko, R. Gaehler, B. Roessli, and P. Boeni, Physica B (Amsterdam) **397**, 125 (2007).
[27] See Supplemental Material at http://link.aps.org/supplemental/10.1103/PhysRevLett.109.017201 for a detailed description of these calculations.
[28] A. Yaouanc, P. Dalmas de Réotier, Y. Chapuis, C. Marin, S. Vanishri, D. Aoki, B. Fåk, L. P. Regnault, C. Buisson, A. Amato, C. Baines, and A. D. Hillier, Phys. Rev. B **84**, 184403 (2011); H. Takatsu, H. Kadowaki, T. J. Sato, Y. Tabata, and J. W. Lynn, J. Phys. Condens. Matter **24**, 052201 (2012).
[29] V. Khemani, R. Moessner, S. A. Parameswaran, and S. L. Sondhi, arXiv:1204.3646.
[30] S. T. Bramwell and M. J. Harris, J. Phys. Condens. Matter **10**, L215 (1998); R. Moessner, Phys. Rev. B **57**, R5587 (1998).